PERGAMON

International Journal of Heat and Mass Transfer 42 (1999) 2905–2920

International Journal of HEAT and MASS TRANSFER

A new approach for the study of turbulent boundary layers with blowing

J. Bellettre, F. Bataille*, A. Lallemand

Centre de Thermique de Lyon, UPRES - A CNRS 5008, INSA de Lyon, 69621 Villeurbanne Cedex, France

Received 16 October 1997; in final form 5 October 1998

Abstract

The study of a turbulent boundary layer submitted to injection through a porous plate is investigated. Using a classical model of turbulence for the main flow, the physical phenomena linked to the blowing are modeled considering the porous plate as a discrete succession of pores and solid elements. The main flow can have a temperature different from that of the injected fluid and both dynamic and thermal aspects have been considered. The results have been compared with results from the literature and with experimental measurements, showing a good agreement. An important decrease in the friction factor with the injection rate has been observed. Furthermore, the heat transfer coefficient decrease is very significant.

Nomenclature

A van Driest constant ($A = 26$)
B blowing factor ($B = F/St$)
B_f blowing factor ($B_f = 2F/C_f$)
C_f friction factor ($C_f/2 = \tau_w/\rho_e U_e^2$)
c_p specific heat [J kg^{-1} K^{-1}]
E friction constant ($E = 9.8$ for a smooth wall)
F injection rate ($F = (\rho U_2)_w/(\rho U_1)_e$)
H enthalpy (mean value) [J kg^{-1}]
h convective heat transfer coefficient [W m^{-2} K^{-1}]
h' enthalpy fluctuation
I turbulence intensity
k turbulent kinetic energy [m^2 s^{-2}]
P pressure [Pa]
p hole diameter [m]
Pr Prandtl number ($Pr = \mu c_p/\lambda$)
q convective heat flux [W m^{-2}]
Re_L Reynolds number ($Re_L = \rho U_{1e} L/\mu$)
St Stanton number ($St = h/\rho U_{1e} c_p$)
T temperature [K]
U velocity (mean value) [m s^{-1}]
u' velocity fluctuation [m s^{-1}]
U^* friction velocity ($U^* = \sqrt{\tau_w/\rho}$) [m s^{-1}]
V^+_w dimensionless vertical velocity ($V^+_w = U_{2w}/U^*$) [m s^{-1}]
x spatial coordinate [m]
y^+ dimensionless coordinate $y^+ = \rho U^* x_2/\mu$.

Greek symbols

Δ enthalpy thickness
$\Delta = \int_0^\infty (\rho U_1/\rho_e U_{1e})(T - T_e)/(T_w - T_e)\,dx_2$ [m]
δ_{ij} Kronecker symbol
ε turbulent kinetic energy dissipation rate [m^2 s^{-3}]
θ momentum thickness
$\theta = \int_0^\infty (\rho U_1/\rho_e U_{1e})[1 - (U_1/U_{1e})]\,dx_2$ [m]
κ Von Karmann constant ($\kappa = 0.44$)
λ thermal conductivity [W m^{-1} K^{-1}]
μ dynamic viscosity [kg m^{-1} s^{-1}]
ν kinematic viscosity [m^2 s^{-1}]
ρ density [kg m^{-3}]
σ_h turbulent Prandtl number
τ shear stress [Pa].

Subscripts

0 without blowing
1 longitudinal direction
2 vertical direction
e main flow
i, j i, j directions
mol molecular
p close to the wall (i.e. at the first node)
t turbulent
w on the wall.

* Corresponding author.

0017–9310/99/$ - see front matter
PII: S0017–9310(98)00341–X

1. Introduction

A turbulent boundary layer submitted to blowing has been the subject of various studies and remains one of the most interesting problems in fluid dynamics and heat transfer. The experimental approaches of Moffat and Kays [1], Simpson et al. [2], Baker and Launder [3] and Romanenko and Kharchenko [4] have given important information and understanding on this topic. Furthermore, the works of Simpson [5], Stevenson [6] or Silva-Feire [7], have permitted the establishment of the modified law of the wall or law of the wake for taking the injection into account. We can also cite the works of Kays [8] and Landis and Mills [9] for modified mixing-length models and the modelisation at low Reynolds numbers with surface heat and mass transfer by So and Yoo [10] and Campolina Franca [11–14].

The main application of blowing is the protection of surfaces such as the nozzle of rocket engines, which are exposed to high temperatures. Other processes have been studied like film cooling [15] or discrete injection [16] for which the surface is a perforated solid (one or several holes) and the coolant fluid flows on the wall surface. We can also envisage the ablation process with a thermally degradable solid added on the wall, that is then protected by the solid sublimation. Nevertheless, problems linked to an important mass flow of coolant fluid to obtain a good efficiency or to a need of periodically renewing of the protector solid, lead to the consideration of blowing as a simple and efficient way to prevent surfaces being exposed to high temperatures. Cooling using blowing does not present these disadvantages and is considered as the most efficient way. In this case, the wall to be protected is made of a porous material and a cold fluid is injected through it.

In this study, we are interested in the numerical aspect of a turbulent boundary layer linked to fluid transfer coming from the porous plate. The configuration of the problem is illustrated in Fig. 1.

Air flows within a 0.2 m high channel at a steady state. The floor is first constituted of an impermeable wall (1.30 m), then of a porous plate (30 cm) where the cold air is injected. The main flow has a longitudinal velocity, U_1, equal to 10 m s^{-1} and the longitudinal turbulent intensity, I, is 1%. The Reynolds number is high enough so that the boundary layer is turbulent before the porous plate. Furthermore, the boundary layer of the developing turbulent flow is two-dimensional. We note x_1 the longitudinal coordinate and x_2 the vertical one (the origin being in the bottom left corner of the channel).

The governing equations of the problem and the numerical method are described. Then, the modeling of the blowing is proposed. Finally, results for cases at ambient temperature, with temperature differences (between the main flow and the injected one) and with different injection rate are presented and discussed.

2. Governing equations and numerical method

2.1. Equations

The governing equations are the continuity, momentum and energy ones where the Reynolds decomposition is applied (decomposition into an average and a fluctuating part). The flow is an ideal gas and there is no gravity effect. Following these procedures, the mean flow equations are given by equations (1)–(3):

$$\frac{\partial \rho U_j}{\partial x_j} = 0 \tag{1}$$

$$\frac{\partial}{\partial x_j}(\rho U_i U_j) = -\frac{\partial P}{\partial x_i} + \frac{\partial}{\partial x_j}\left(\mu\left[\frac{\partial U_i}{\partial x_j} + \frac{\partial U_j}{\partial x_i}\right] - \frac{2}{3}\mu\frac{\partial U_i}{\partial x_i} - \rho\overline{u_i' u_j'}\right) \tag{2}$$

$$\frac{\partial}{\partial x_j}(\rho U_j H) = \frac{\partial}{\partial x_j}\left(\lambda\frac{\partial T}{\partial x_j}\right) - \frac{\partial}{\partial x_j}(\rho\overline{u_j' h'}) + U_j\frac{\partial P}{\partial x_j} \tag{3}$$

where U, H and P are the mean values of velocity,

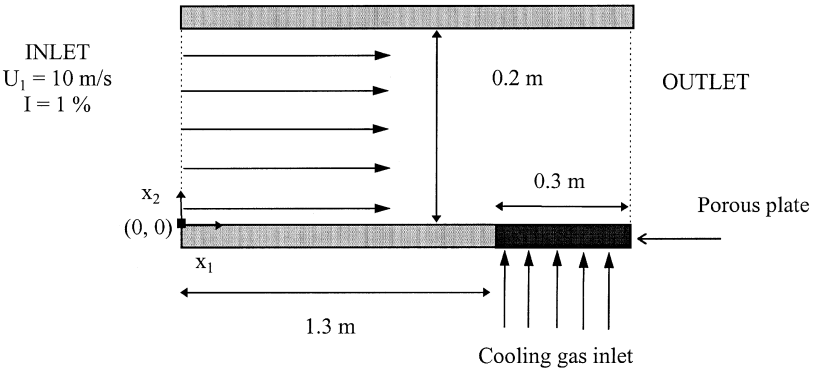

Fig. 1. Studied configuration.

enthalpy and pressure, u' and h' the velocity and enthalpy fluctuations, ρ the fluid density, μ the dynamic viscosity and λ the thermal conductivity. In these equations, μ and λ are temperature dependent and ρ follows the ideal gas law (the fluid density varies from 0.95 to 1.2 kg m^{-3}).

The aim of this study is not to develop a new model of turbulence with injection but to use a classical model of turbulence and to model the injection. In a first time, we consider two classical models of turbulence: the standard k–ε model and the Renormalisation Group k–ε model (RNG k–ε). As the objective is not to describe these models, only the main part and the useful equations will be given by the following. More information and details can be found in [17, 18]. These two models will be tested by comparing with experimental data, and the most adapted model for our case will be kept.

2.1.1. *Standard* k–ε *model* [17]

The turbulent Reynolds stresses appearing in the main flow equations are modeled using a turbulent viscosity v_t:

$$\overline{u_i'u_j'} = -v_t\left(\frac{\partial U_i}{\partial x_j}+\frac{\partial U_j}{\partial x_i}\right)+\frac{2}{3}v_t\frac{\partial U_i}{\partial x_i}\delta_{ij}+\frac{2}{3}k\delta_{ij}$$

and

$$\overline{u_j'h'} = -\frac{v_t}{\sigma_h}\frac{\partial c_p T}{\partial x_j}$$

with $\sigma_h = 0.7$ (turbulent Prandtl number). v_t is determined by k, the turbulent kinetic energy and ε, the dissipation rate of k, according to the relation (4):

$$v_t = C_\mu\frac{k^2}{\varepsilon} \tag{4}$$

with $C_\mu = 0.09$.

Furthermore, k and ε are obtained from the solution of their respective transport model (equations (5) and (6)):

$$\frac{\partial(\rho U_j k)}{\partial x_j} = \frac{\partial}{\partial x_j}\left(\frac{\rho v_t}{\sigma_k}\frac{\partial k}{\partial x_j}\right)+\rho v_t\left(\frac{\partial U_i}{\partial x_j}+\frac{\partial U_j}{\partial x_i}\right)\frac{\partial U_i}{\partial x_j}-\rho\varepsilon \tag{5}$$

$$\frac{\partial(\rho U_j \varepsilon)}{\partial x_j} = \frac{\partial}{\partial x_j}\left(\frac{\rho v_t}{\sigma_\varepsilon}\frac{\partial \varepsilon}{\partial x_j}\right)+C_{\varepsilon 1}\frac{\varepsilon}{k}\rho v_t\left(\frac{\partial U_i}{\partial x_j}+\frac{\partial U_j}{\partial x_i}\right)\frac{\partial U_i}{\partial x_j} - C_{\varepsilon 2}\rho\frac{\varepsilon^2}{k} \tag{6}$$

with $\sigma_\varepsilon = 1.3$, $\sigma_k = 1.0$, $C_{\varepsilon 1} = 1.44$ and $C_{\varepsilon 2} = 1.92$.

2.1.2. *Renormalisation Group* k–ε *model*

The RNG k–ε model extends the prediction of the turbulent viscosity. The assumptions and the improvement of this model can be found in Yakhot and Orszag [18]. Several versions of the RNG k–ε have been developed and an overview of the differences between the RNG k–ε models can be found in Zhou et al. [19]. In this work, we used the recent development of Yakhot and Orszag [19] where the resulting equations are the following:

$$\frac{\partial(\rho U_j k)}{\partial x_j} = \frac{\partial}{\partial x_j}\left[\alpha_k\rho v_{\text{eff}}\frac{\partial k}{\partial x_j}\right]+\rho v_t\left(\frac{\partial U_i}{\partial x_j}+\frac{\partial U_j}{\partial x_i}\right)\frac{\partial U_i}{\partial x_j}-\rho\varepsilon \tag{7}$$

$$\frac{\partial(\rho U_j \varepsilon)}{\partial x_j} = \frac{\partial}{\partial x_j}\left(\alpha_\varepsilon\rho v_{\text{eff}}\frac{\partial \varepsilon}{\partial x_j}\right) + C_{\varepsilon 1}\frac{\varepsilon}{k}\rho v_t\left(\frac{\partial U_i}{\partial x_j}+\frac{\partial U_j}{\partial x_i}\right)\frac{\partial U_i}{\partial x_j} - C_{\varepsilon 2}\rho\frac{\varepsilon^2}{k} - R \tag{8}$$

with

$$v_{\text{eff}} = v_{\text{mol}}\left(1+\sqrt{\frac{C_\mu}{v_{\text{mol}}}}\frac{k}{\sqrt{\varepsilon}}\right)^2 = v_{\text{mol}}\left(1+\sqrt{\frac{v_t}{v_{\text{mol}}}}\right)^2$$

(v_{mol} being the molecular kinetic viscosity), $C_\mu = 0.0845$, $C_{\varepsilon 1} = 1.42$ and $C_{\varepsilon 2} = 1.68$. α_k and α_ε are the inverse turbulent Prandtl numbers for k and ε. In the high Reynolds domain $\alpha_k = \alpha_\varepsilon = 1.39$. At last,

$$R = \frac{C_\mu\rho\eta^3\left(1-\dfrac{\eta}{4.38}\right)}{1+0.012\eta^3}\frac{\varepsilon^2}{k}$$

with $\eta = Sk/\varepsilon$, where S is the modulus of the tensor S_{ij},

$$S_{ij} = \frac{1}{2}\left(\frac{\partial U_j}{\partial x_i}+\frac{\partial U_i}{\partial x_j}\right).$$

2.2. Boundary conditions

In the k–ε and RNG k–ε models, the near wall effect is taken into account by the Launder and Spalding logarithmic-law of the wall, equation (9), used under condition of equilibrium [20]:

$$\frac{U}{U^*} = \frac{1}{\kappa}\ln(Ey^+) \quad \text{for } 11.2 < y^+ < 100 \tag{9}$$

and where

$$U^* = \sqrt{\frac{\tau_w}{\rho}} = C_\mu^{1/4}k_p^{1/2}$$

τ_w is the wall shear stress, κ is the von-Karman's constant, E is an empirical constant set equal to 9.8 (smooth wall) and

$$y^+ = \frac{\rho U^* x_2}{\mu} = \frac{\rho C_\mu^{1/4}k_p^{1/2}x_2}{\mu}.$$

k_p, the near wall value of k (i.e. at the first node of the grid), is determined by solving, in the wall-adjacent cell, the transport equation for k (equations (5) or (7)) with a zero normal gradient assumed at the wall for boundary condition.

The boundary condition for ε (ε_p) is given by the equilibrium assumption (production and dissipation of tur-

bulent kinetic energy are equal) implying relation (10) at the first node of the grid:

$$\varepsilon_p = \frac{C_\mu^{3/4} k_p}{\kappa x_{2p}} \tag{10}$$

(x_{2p} being the nearest wall point in vertical coordinate).

For the thermal boundary conditions on the wall, the Launder and Spalding [20] logarithmic-law of the wall, equation (11) is used:

$$\frac{\rho c_p \Delta T C_\mu^{1/4} k_p^{1/2}}{q} = \frac{\sigma_h}{\kappa}\ln(Ey^+) + \sigma_h\left(\frac{\sigma_h}{Pr}\right)^{1/4}\frac{\pi/4}{\sin(\pi/4)}\left(\frac{A}{\kappa}\right)^{1/2}\left(\frac{Pr}{\sigma_h}-1\right) \tag{11}$$

where q is heat transfer at the wall, $\Delta T = T_w - T_p$, Pr the fluid Prandtl number, σ_h the turbulent Prandtl number (0.85 near the wall) and A the van Driest constant ($A = 26$). T_w can be either fixed or calculated according external heat transfer boundary conditions.

2.3. Numerical method

The numerical procedure is based on a finite volume approach with quadrilateral control volumes and structured meshes. The diffusion terms are discretized according to a central difference method and the convective terms using a power law scheme [21]. Pressure velocity coupling is calculated with the SIMPLE cell-centered scheme [21]. The discrete algebraic equations are solved using a line-by-line tri-diagonal matrix [22].

The grid is cartesian and several resolutions have been tested. In the longitudinal direction, the grid is linear and different tests showed that the results are independent of the cell lengths (between 5 and 50 mm). In the vertical direction the grid can be either linear or with a geometrical progression. It has been observed that the numerical results are independent of the grid kind and of the vertical space step (included between 0.75 and 3 mm) for a linear grid. It can be noticed that the laws of the wall, equations (9) and (11), are used only for the first point over the wall. This point is always fixed in order to remain in the validity domain of the laws without going in the laminar sublayer ($y^+ > 11.2$).

Furthermore, the convergence of the results are tested according to two criteria. First, all the normalized residuals must be less than 10^{-4} knowing that the normalization of the residuals is calculated in function of the mean value of the considered variable at each iteration [22]. Secondly, supplementary iterations do not change the calculation results (the evolution is less than 0.5%).

2.4. Choice of the turbulence model

In order to select the most adapted model to our geometry and to validate our numerical method, we tested the k–ε and RNG models to simulate the turbulent flow before the porous plate, in the configuration showed in Fig. 1. The objective is to see the differences between these two models in our case without injection even if, for such a classical flow, the two models results should be very close. We will use the turbulence model to represent the turbulent flow and to separately model the blowing.

2.4.1. Velocity profiles and friction factors

The comparisons are done, for the velocities, with experimental data from the test channel of our laboratory, the velocities being measured by laser Doppler Anemometry [23]. The boundary conditions at the channel inlet are uniform U_1 fixed at 10 m s^{-1}, uniform k and ε deduced from the turbulence intensity ($k = 0.015$ m^2 s^{-2} and $\varepsilon = 0.03$ m^2 s^{-3}). The longitudinal velocity U, as a function of x_2, is represented in Fig. 2 for a Reynolds number $Re_{x1} = 856\,000$, corresponding to $x_1 = 1.25$ m. We can observe that the RNG calculations and experimental data match very well. The standard k–ε model gives rather accurate results but its curve cuts across the experimental one. According to this first result, the RNG model seems to be a bit more adapted than the k–ε one.

Furthermore, we are interested in the friction factor which is defined by relation (12):

$$\frac{C_{f0}}{2} = \frac{\tau_w}{\rho_e U_e^2} \tag{12}$$

For the standard k–ε and RNG k–ε models coupled with the law of the wall, the skin coefficient is determined using the semi-empirical relation under equilibrium condition [20].

$$U^* = \sqrt{\frac{\tau_w}{\rho_w}} = C_\mu^{1/4} k_p^{1/2} = U_e\sqrt{\frac{\rho_e}{\rho_w}}\sqrt{\frac{C_{f0}}{2}}.$$

In Fig. 3, we plot the friction factor in function of the Re_{x1}, in a range of variation from 4.5×10^5–8.5×10^5. This friction factor is compared to the Blasius correlation (13) confirmed by Moffat and Kays [1] and Romanenko and Kharchenko [4] experiments:

$$\frac{C_{f0}}{2} = aRe_{x1}^{-0.2} \quad \text{with} \quad a = 0.0295 \tag{13}$$

We can see that the results given by the RNG k–ε model are very close to the Blasius correlation. As in the first test, the standard k–ε model gives close results (about 5% lower). We can suppose that the discrepancy is only a consequence of a different value of the C_μ constant and k_p calculation. The RNG k–ε model seems to be the most adapted to our study and will be retained in the following. Nevertheless, we tested this model including heat transfer phenomena and for results obtained with integral correlations.

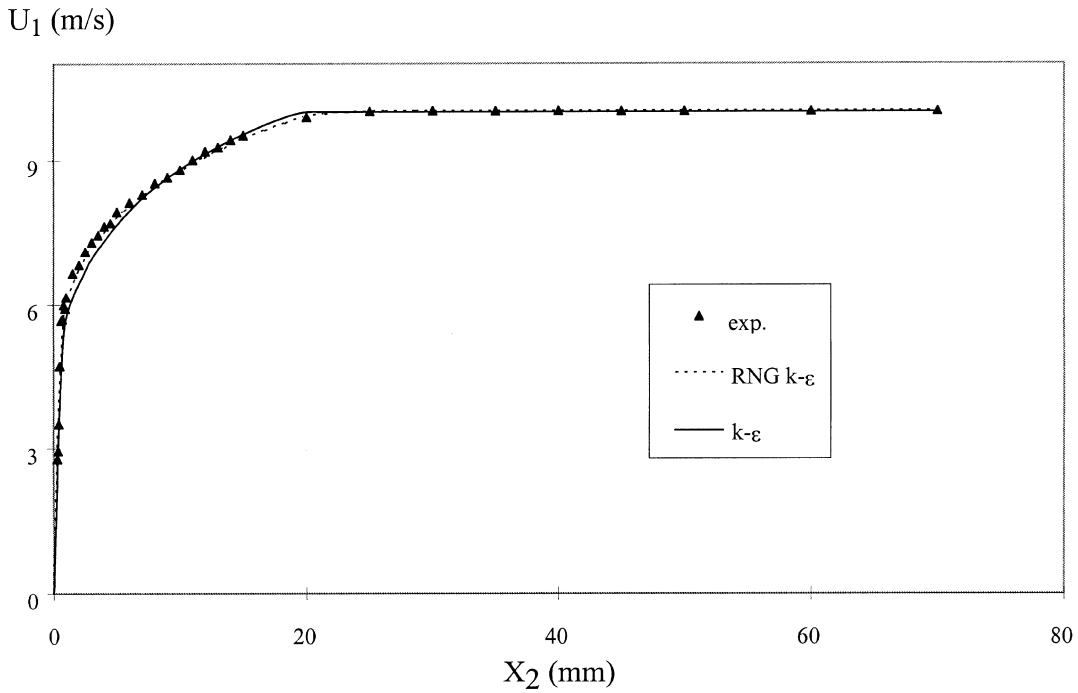

Fig. 2. Experimental and calculated velocities without injection.

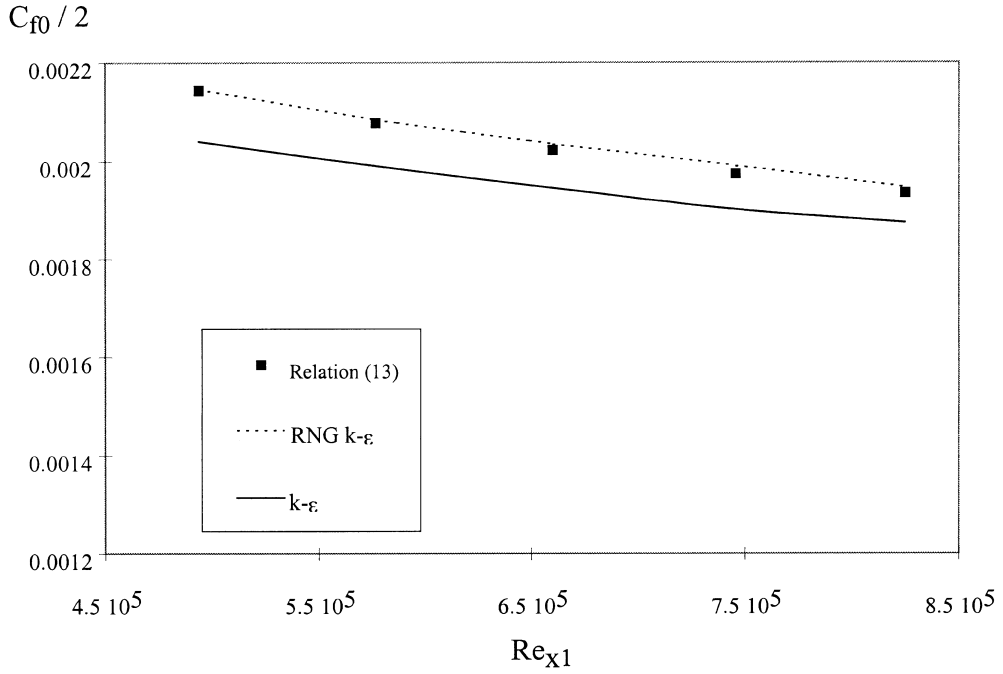

Fig. 3. Friction factor with Re_{x1} between 4.5×10^5 and 8.5×10^5.

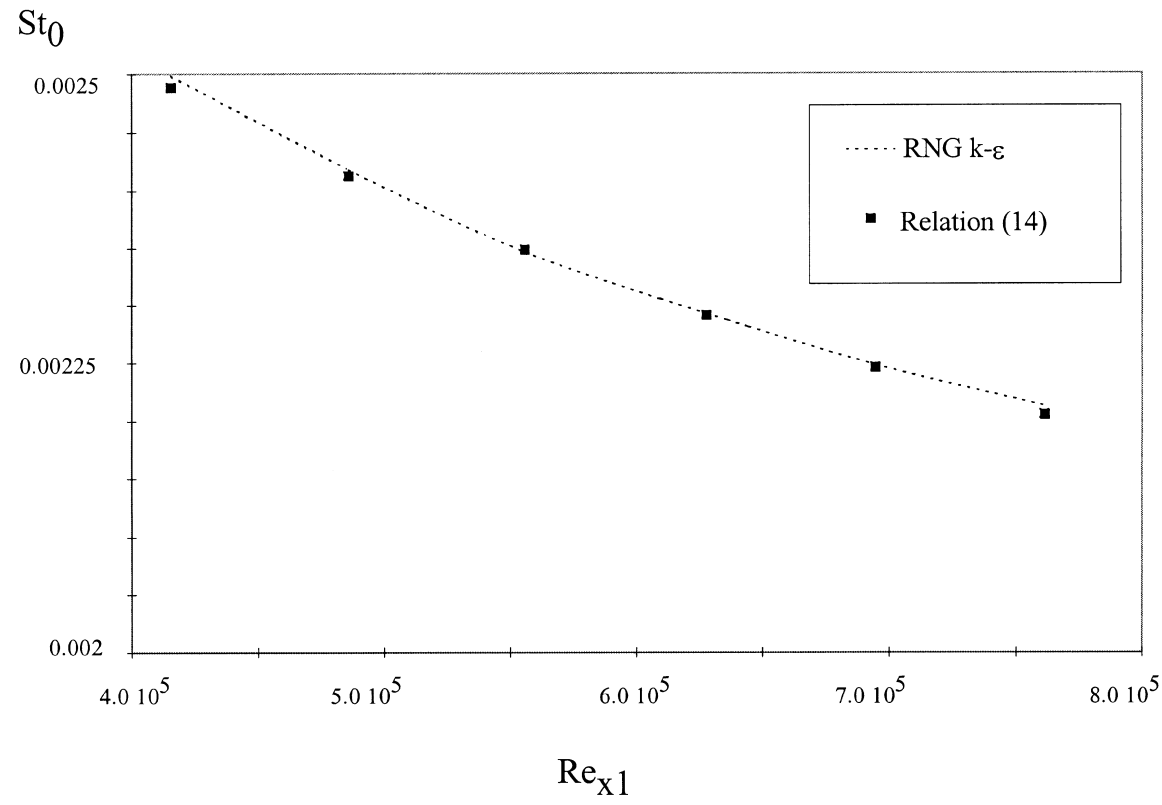

Fig. 4. Stanton number with Re_{x1} between 4×10^5 and 8×10^5.

2.4.2. Heat transfer

We tested the RNG k–ε model for the thermal transfers between a hot turbulent boundary layer and the impermeable wall. The flow has a temperature of 45°C and the wall temperature is fixed to 35°C. Moffat and Kays [1] results, in terms of convective heat flux, are correlated by the relation (14):

$$St_0 = \frac{q}{\rho_e c_p U_{1e}(T_e - T_w)} = 0.0295 Re_{x1}^{-0.2} Pr^{-0.4} \qquad (14)$$

In Fig. 4, the results, obtained with this correlation and the simulation using the RNG k–ε model where the flux is calculated according the relation (11)—k_p being computed with equation (7)—are given. We can observe that the results are in very good agreement and that the RNG k–ε model always seems to be adapted.

2.4.3. Comparisons model—integral correlations

Furthermore, as we will use integral correlations, we compared the friction factor and the Stanton number calculated by RNG k–ε model and by integral correlations.

For the friction factor, we involve the correlation taking into account the Reynolds number based on the momentum thickness. Simpson et al. [2] proposed the relation (15) and Andersen et al. [24], the relation (16). The coefficients of these two correlations have been experimentally determined. Nevertheless, the results of Simpson et al. [2] seem to be too high according to Squire [25]:

$$\frac{C_{f0}}{2} = aRe_\theta^{-0.25}, \quad \text{with } a = 0.013 \qquad (15)$$

$$\text{with } a = 0.012 \qquad (16)$$

The comparison between these correlations and the results obtained with the RNG k–ε model, at ambient temperature, are shown in Fig. 5. In the RNG k–ε case, the friction factor has been determined according to the relation (12), where the wall shear stress is computed under condition of equilibrium. In the integral correlations cases, the Reynolds number has been calculated by integrating the numerical profile of longitudinal velocity in the boundary layer. We can notice that the results of Andersen's correlation are very close to our model.

In the same way, we calculate the convective heat flux between the hot flow and the wall using the Reynolds number based on the enthalpy thickness. Whitten et al. [26] propose the relation (17), obtained for a weak temperature difference between the main flow and the wall:

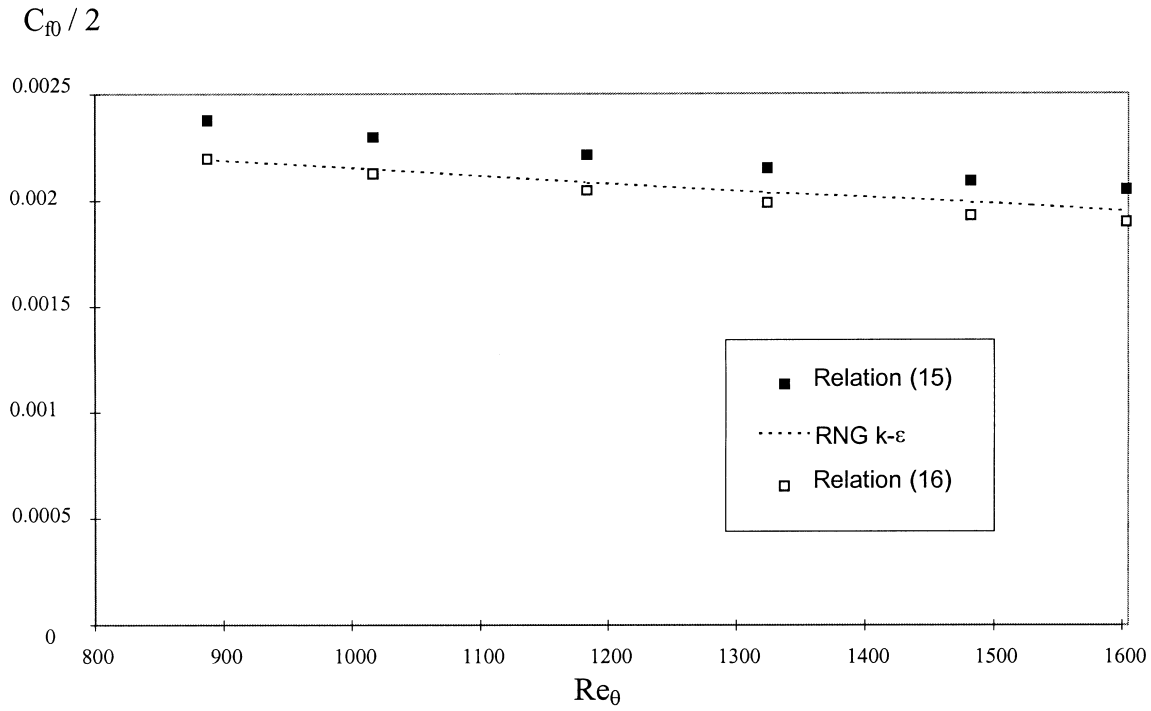

Fig. 5. Friction factor with Re_θ between 800 and 1600.

$$St_0 = 0.0128 Re_\Delta^{-0.25} Pr^{-0.5} \quad (17)$$

We can see in Fig. 6 that the results of the RNG k–ε model (the flux being calculated according the relation (11)) are in good agreement with the relation (17), where the enthalpy thickness is calculated by integrating the velocity and temperature profiles in the boundary layer.

According to all these results without blowing, the RNG k–ε model seems to be very well adapted to our flow configuration. In the framework of our study, we could test other models for the turbulent flows [27] but it is not the objective of this work. In the following, we will use the RNG k–ε model for the main flow and investigate the study of the turbulent boundary layer with blowing.

3. Modeling of the blowing through the porous plate

In order to model the fluid injection through the porous plate, we analyze the phenomenon, to which the turbulent boundary layer is submitted, as a succession of wall shear stress and injected fluid source.

In opposition to other authors [5–7, 11] who take into account the injection by modifying the modelisation of the flow (wall law or introduction of constants in a low Reynolds model), we choose to model the physical phenomenon that occurs when there is injection through a porous plate. This method permits the avoidance of a supplementary empirical law in order to take into account the injection.

For this modeling, we represented the porous plate by a two-dimensional succession of two different kinds of elements. The first is assimilated to a wall which is governed by a classical law of the wall, the second is considered as a source from which a fluid quantity comes. This fluid is laminar, at a given velocity and temperature, and follows the classical law of a laminar motion. The boundary conditions for the hole are fixed temperature and vertical velocity (U_2); k and ε are equal to zero. The acceleration of the fluid, inside the porous plate, has been taken into account in the calculation of the boundary condition on the vertical velocity (U_2 at the pore exit is determined by considering the fluid mass flow and the cross section inside the plate).

Consequently, the boundary layer submitted to blowing results in the mixing of two flows (main flow plus laminar flow injection). The source fluid modifies the main flow by bringing a given mass and a given heat quantity, that is transported by convection and conduction. At the same time, this mixing is submitted to the shear stress.

Different element succession ratios have been tested. The first configuration is an alternated succession of the two elements in a proportion of one third of holes and two thirds of wall (Fig. 7). These proportions have been chosen in order to be as close as possible to the porosity

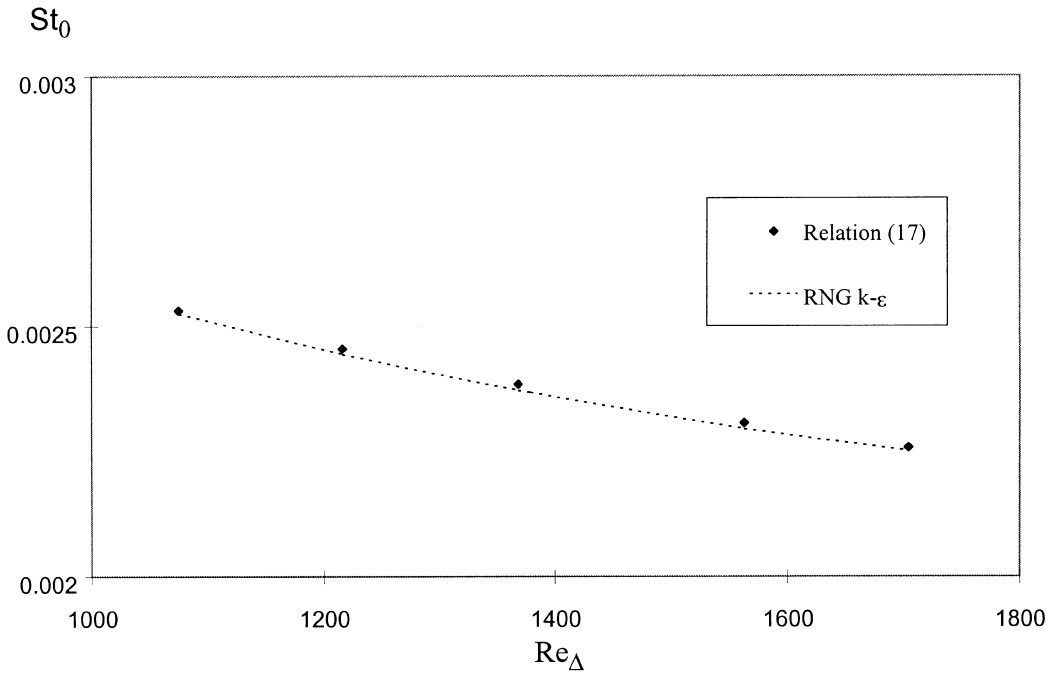

Fig. 6. Stanton number with Re_Δ between 1000 and 1800.

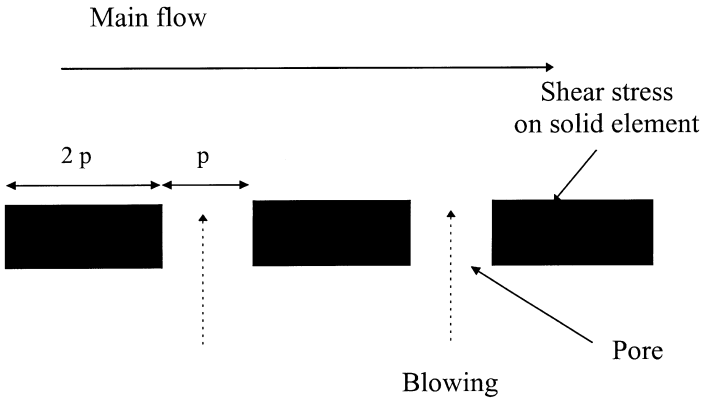

Fig. 7. Model of porous plate model.

of the porous plate used in our test channel [23] (around 30% porosity). The following results will be given in this configuration but the influence of the proportion is investigated in Section 4.2.4.

The discretisation step (length of a hole) has been fixed to 2.5 mm. However, we studied the sensibility of the hole size, knowing that the real porous plate has holes of 30 μm of diameter and is three-dimensional. For a range size varying from 1 to 5 mm, we could observe that the calculations were not affected. In this range, the effects due to the wall and to the injection through the pores are independent of the discretisation step under the condition of keeping a constant porosity and a constant injected mass flow.

In order to illustrate the effects of the wall shear stress and of the holes, we plotted in Fig. 8 the longitudinal velocity profile obtained, at $x_1 = 1.56$ m, with only wall (no injection, characterizing only the friction) and with only pores (constant vertical velocity on all the length and longitudinal velocity equal to zero). These two profiles are compared with experimental results obtained with injection. It clearly appears that the two phenomena influence the boundary layer and that they both need to be taken into account in the model.

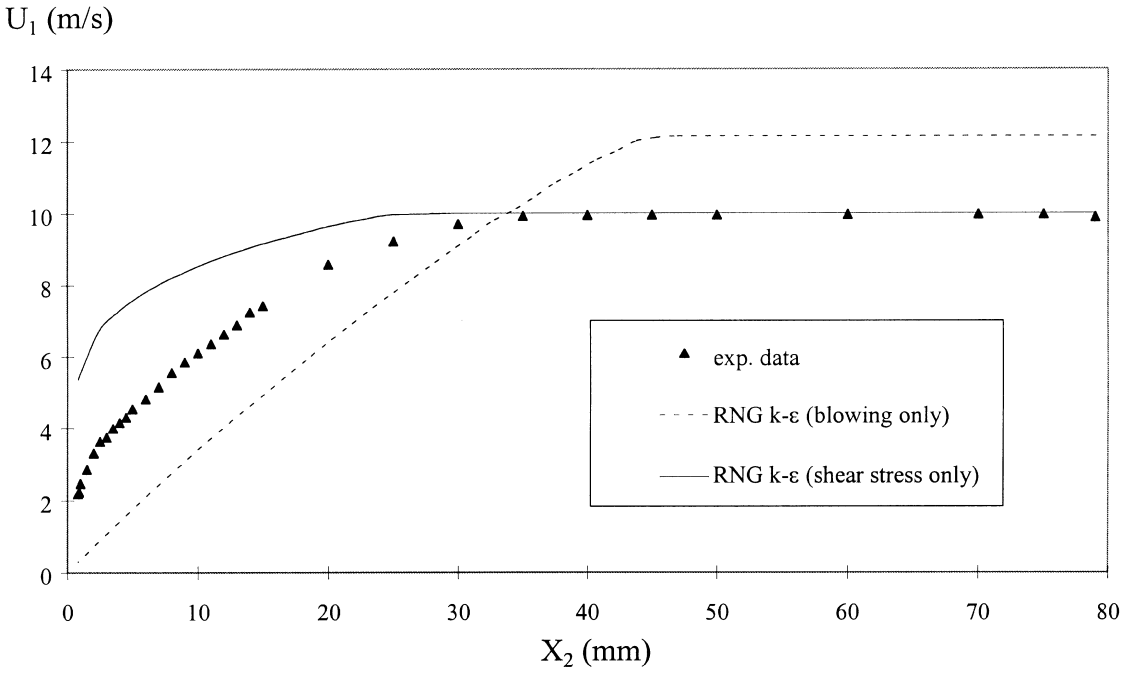

Fig. 8. Velocities in near the end of porous plate ($x_1 = 1.56$ m).

4. Results

4.1. Study of the flow with injection at the same temperature

Using the RNG k–ε model and the model of the injection through a porous plate, we consider the case of an injection rate of 1%, the main flow and the injected fluid being at the same temperature.

We are first interested in the longitudinal velocity and in the friction factor. The results obtained are compared with our experimental results [23] and with different results of the literature. We can observe in Fig. 9 that the velocity profile, as a function of x_2, is very affected by the injection and that the boundary layer thickness increases by about 50%. We can note that our results are in very good agreement with the experimental results before the injection and in the injection region (i.e. at the end of the porous plate).

In Fig. 10, the dimensionless velocity is plotted and compared to the law of the wall with injection of Simpson [5] (equation (18)):

$$\frac{2}{V_w^+}\left[\left(1+V_w^+\frac{U_1}{U^*}\right)^{0.5}-(1+11V_w^+)^{0.5}\right]=\frac{1}{\kappa}\ln\left(\frac{y^+}{11}\right) \tag{18}$$

with

$$V_w^+=\frac{U_{2w}}{U^*},$$

U_{2w} being the vertical velocity at the wall and U^* is deduced from relation (19).

The experimental and RNG curves are closed the one to the other and Simpson's law of the wall is respected for $30 < y^+ < 100$, which corresponds to the validity domain of this law [5].

Concerning the friction factor, C_f, we calculate C_f before injection and in the injection region (i.e. near the end of the porous plate, $x_1 = 1.56$ m) using the Simpson et al. [2] correlation (19) where C_{f0} is determined by the Andersen et al. relation (16).

$$\left.\frac{C_f}{C_{f0}}\right|_{Re_\theta}=\left[\frac{\ln(1+B_f)}{B_f}\right]^{0.7}, \quad \text{with injection} \tag{19}$$

with $B_f = 2F/C_f$ and for $0.2 < 1+B_f < 65$.

The momentum thickness θ is evaluated by discrete integration of the experimental or numerical data. The blowing factor B_f in the injection region is 23 i.e. in the middle of the interval of validity. Table 1 shows all the friction factor calculations (for both regions, the left column calculations are done with the experimental velocities and the right with the calculated ones).

The differences between the friction factors calculated with experimental or RNG k–ε data are less than 5% in both regions. The comparison between friction factors

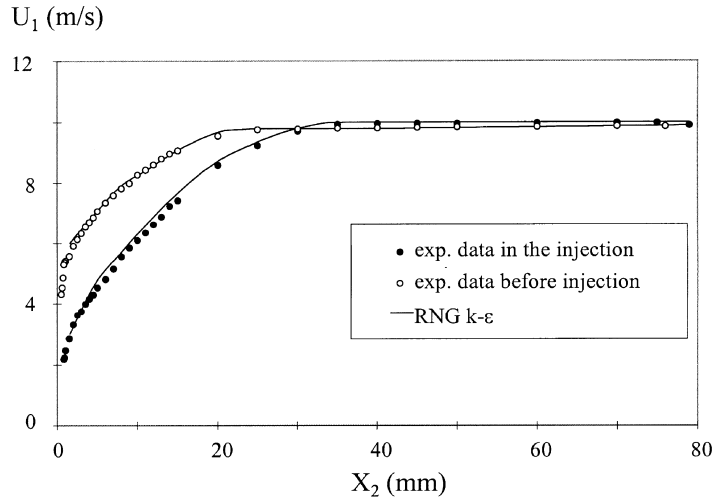

Fig. 9. Longitudinal velocities before ($x_1 = 1.25$ m) and in the injection region ($x_1 = 1.56$ m).

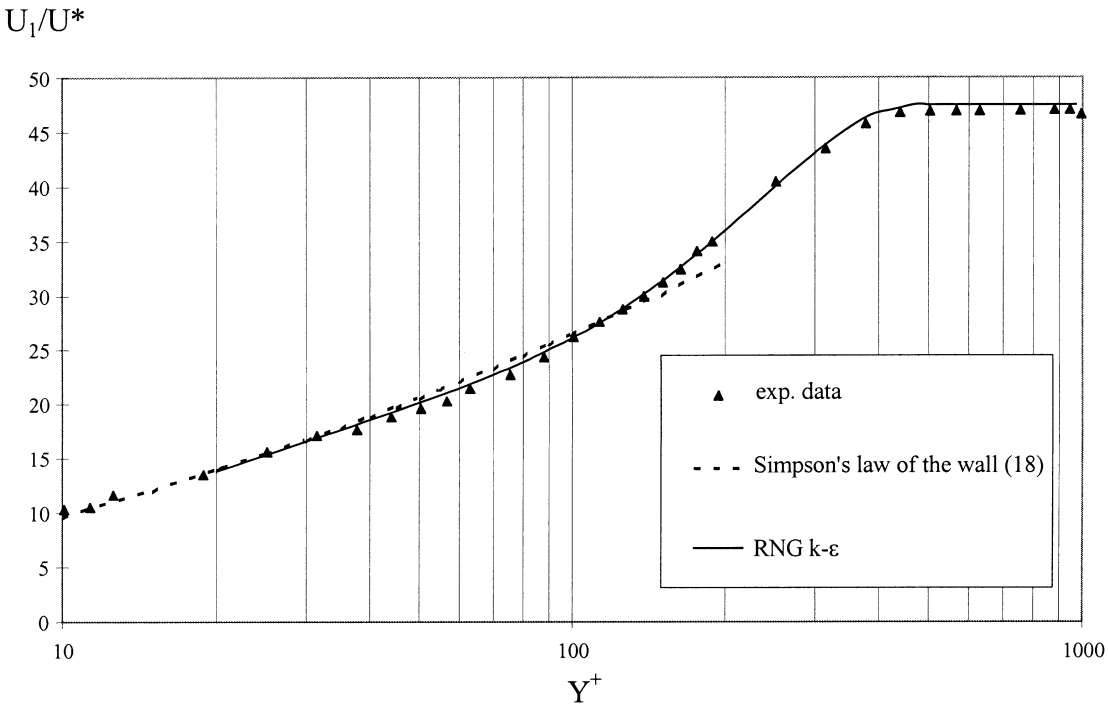

Fig. 10. Dimensionless velocity profile in the injection region.

with and without injection confirms the fact that the friction factor decreases much with injection.

4.2. Study of the flow with injection at different temperatures

In this part, we increase the temperature of the main flow to 45 and 100°C. The mass flow of cold gas through the porous plate is equal to that of the ambient case. The temperatures of the injected gas and of the solid element of the porous plate are supposed to be equal (hypothesis of thermal equilibrium between fluid and solid at the exit of the porous plate). The value of this temperature is given by experimental measurement [23] and is equal to 31°C for a main flow temperature of 45°C, and to 45°C for a main flow temperature of 100°C. The temperature

Table 1
Friction factor ($\times 1000$)

	Before injection ($x_1 = 1.25$ m)		In the injection region ($x_1 = 1.56$ m)	
	Experimental data	RNG k–ε calculations	Experimental data	RNG k–ε calculations
Relation (19)	1.87	1.82	0.42	0.40

of the impermeable plate before the injection region is calculated taking into account the heat transfer with the external medium.

4.2.1. Velocity profiles

Longitudinal velocity profiles before injection and in the injection region are calculated and compared to experimental data [11, 23]. The results for temperatures of 45 or 100°C are the same as in the ambient case (Fig. 9).

4.2.2. Temperature profiles

The thermal boundary layers before injection and in the injection region (at the end of the porous plate) are plotted in Fig. 11 respectively for main flow temperatures of 45 and 100°C. The discrepancies between RNG k–ε calculations and experimental data is weak. As in the dynamic boundary layer, the thermal boundary layer increases a lot with injection and therefore heat transfer is reduced and the plate is protected.

4.2.3. Friction factors and Stanton numbers

For both configurations, friction factors and Stanton numbers are calculated in the injection region. Friction factors are determined using the Simpson et al. correlation (equation (19)). Stanton numbers are calculated according to the Whitten et al. [26] correlation (equation (20)), where St_0 is defined by relation (17):

$$\left.\frac{St}{St_0}\right|_{Re_\Delta} = \left[\frac{\ln(1+B)}{B}\right]^{1.25} (1+B)^{0.25} \tag{20}$$

with $B = F/St$.

The enthalpy thickness, Δ, is evaluated by a discrete

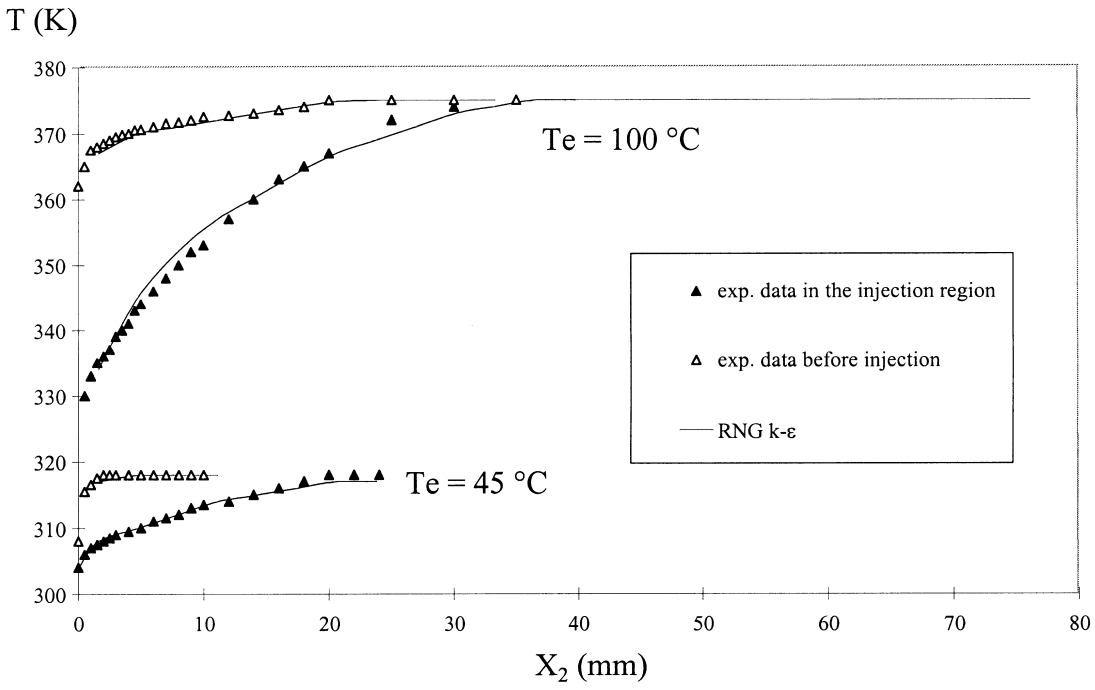

Fig. 11. Thermal boundary layer for 45 and 100°C main flow temperatures.

Table 2
Friction factors and Stanton numbers in the injection region, $x_1 = 1.56$ m ($\times 1000$)

	Ambient temperature		45°C		100°C	
	Experimental data	RNG results	Experimental data	RNG results	Experimental data	RNG results
Cf/2	0.42	0.40	0.39	0.38	0.39	0.38
St	—	—	0.28	0.29	0.29	0.27

integration of experimental or numerical data. We can note that the case at 45°C corresponds to the experimental conditions of Whitten et al. [26]. At 100°C, it is possible to use the same relation (20).

Table 2 gives friction factors and Stanton numbers for the different main flow temperatures at the end of the porous plate. Calculations are performed using experimental data (left column) or RNG results (right column). The differences between friction factors or Stanton numbers calculated with experimental or RNG data are less than 5%.

4.2.4. Effect of the porosity

In this part, we study the influence of the proportion between holes and walls. In all previous results, we took two third of wall and one third of holes in order to respect the value of the porous plate porosity (30%). Nevertheless, it was important to check out if the results are influenced by the chosen proportion.

We tested different ratios of wall equal to 1/4, 1/2, 2/3 (keeping a constant injected flow) and we compared the cases both for the velocity and for the temperature profiles. We can see in Figs 12 and 13 that the dynamic boundary layer is not modified for the values varying from 1/4 to 1/2 (even if the chosen value of 1/3 for our complete study seems to be well adapted to the experimental study [11, 23]). However, the value of 2/3 weakly modifies the velocity profile. Concerning the temperature profile (main flow temperature at 100°C), the same tendency is observed: weak discrepancy for ratio comprised between 1/4 and 1/2 but a difference is noted for a ratio equal to 2/3. Consequently, we can conclude that the proportion between holes and walls does not need to be very precisely determined but has an influence if it is very different from the porous plate actual porosity. If the ratio between blowing and shear stress varies in a large scale, the boundary layers will be affected (cf. Fig. 8 for the limits of 0 and 100% porosity).

4.2.5. Effect of the injection rate

In this part, we evaluate the effect of the injection rate, *F*. This study is done for the ambient case, and for main flow temperatures equal to 45 and 100°C.

The evolution of the friction factor (calculated according the relation (19)) as a function of the injection rate is shown in Fig. 14. A classical decrease in the friction factor with the injection rate is found and we can note that these results are close to experimental data [3, 24, 28]. Comparisons are made for equivalent boundary layer configurations, i.e. experimental Reynolds numbers based on momentum thickness are equal to those of our simulations.

For the 45°C case, calculated Stanton numbers, for different injection rates, are close to the experimental data of Whitten et al. [26] for equivalent enthalpy thickness Reynolds numbers (Fig. 15). Consequently, these results allow to conclude that our blowing model, for different injection rates, is always valid. The deduced convective heat transfer coefficients between the porous plate and the main flow show that, for an injection rate of 1%, the coefficient is reduced by more that 80%, showing the good efficiency of this kind of protection.

In the 100°C case, dimensionless velocity profiles are given in Fig. 16. For the heat transfer aspect, comparable conclusions are made: the thermal protection is very efficient for an injection rate of 1% (for this value, the decrease in the heat transfer coefficient reaches 85% of the value without blowing—Fig. 17). Nevertheless, it is interesting to notice that the blow off of the thermal boundary layer, corresponding to a Stanton number equal to zero, will appear for a slightly higher injection rate.

5. Conclusions

Starting from a classical model of turbulence (RNG k–ε) and modeling the physical phenomena linked to blowing numerical simulations of turbulent fluid flowing on a porous plate submitted to blowing have been successfully carried out. The main flow can have a temperature different to that of the injected fluid and both dynamic and thermal aspects have been considered. The obtained results have been compared with the literature and experimental measurements, showing a good agreement. An important increase in the turbulent boundary

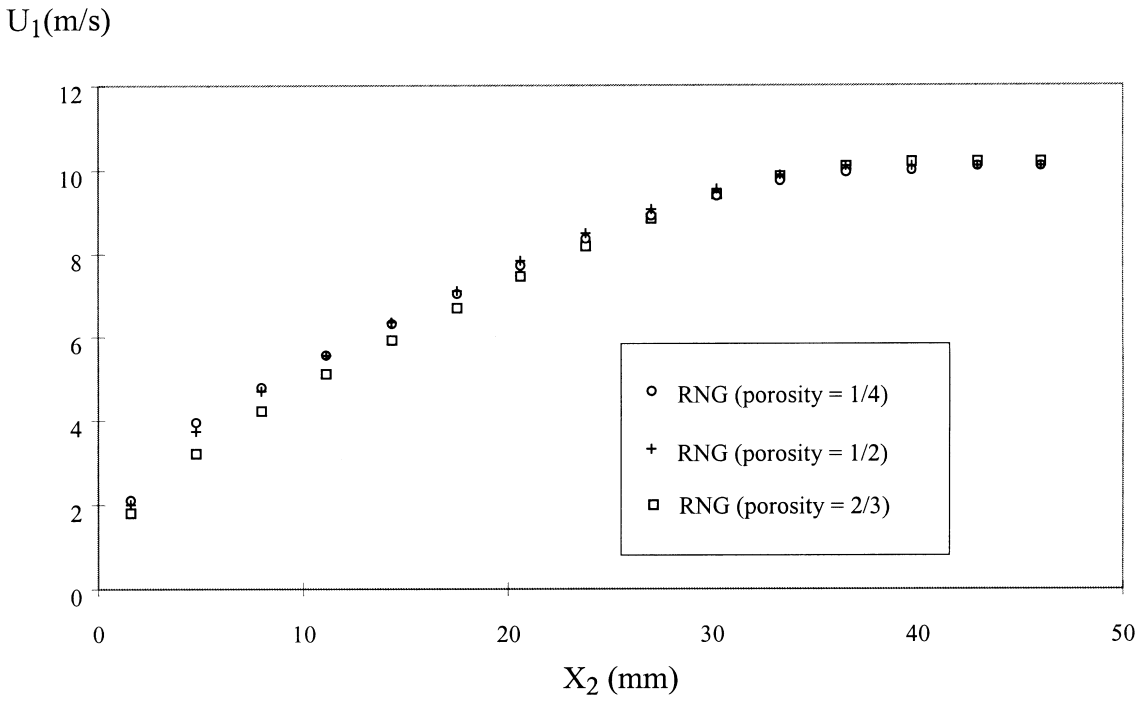

Fig. 12. Effect of porosity on the dynamic boundary layer in the injection region.

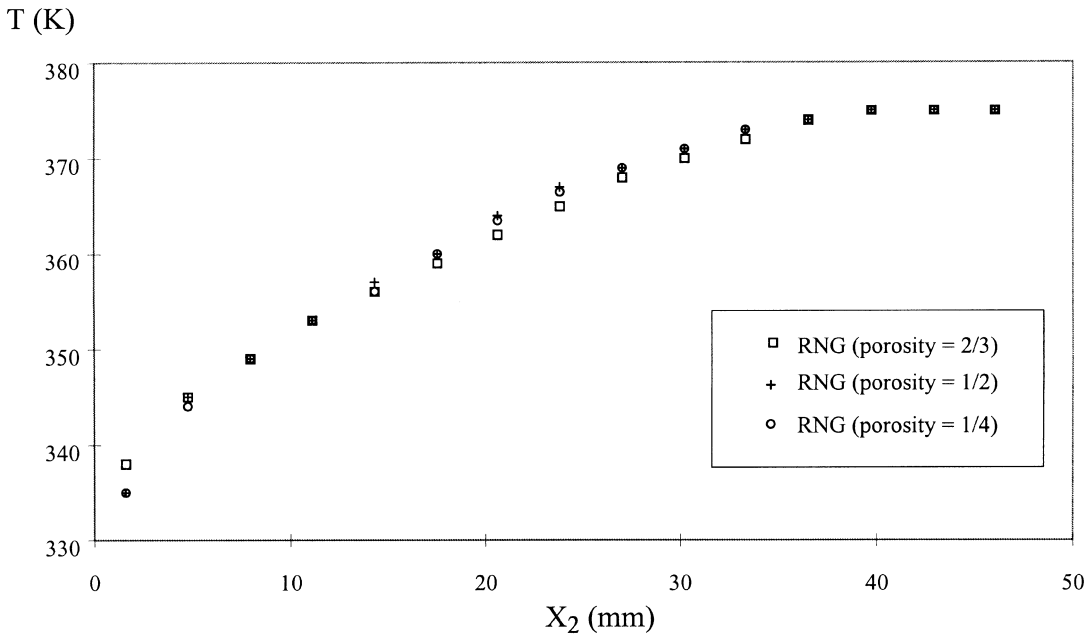

Fig. 13. Effect of porosity on the thermal boundary layer in the injection region.

layer, and an important decrease in the friction factor have been observed. Furthermore, a reduction of the temperature near the wall has been pointed out and the decrease in the heat transfer coefficient is very significant.

This model of turbulent boundary layer submitted to blowing will be linked to a model of heat transfer inside the porous plate [29] in order to study all the phenomena existing in the blowing cooling.

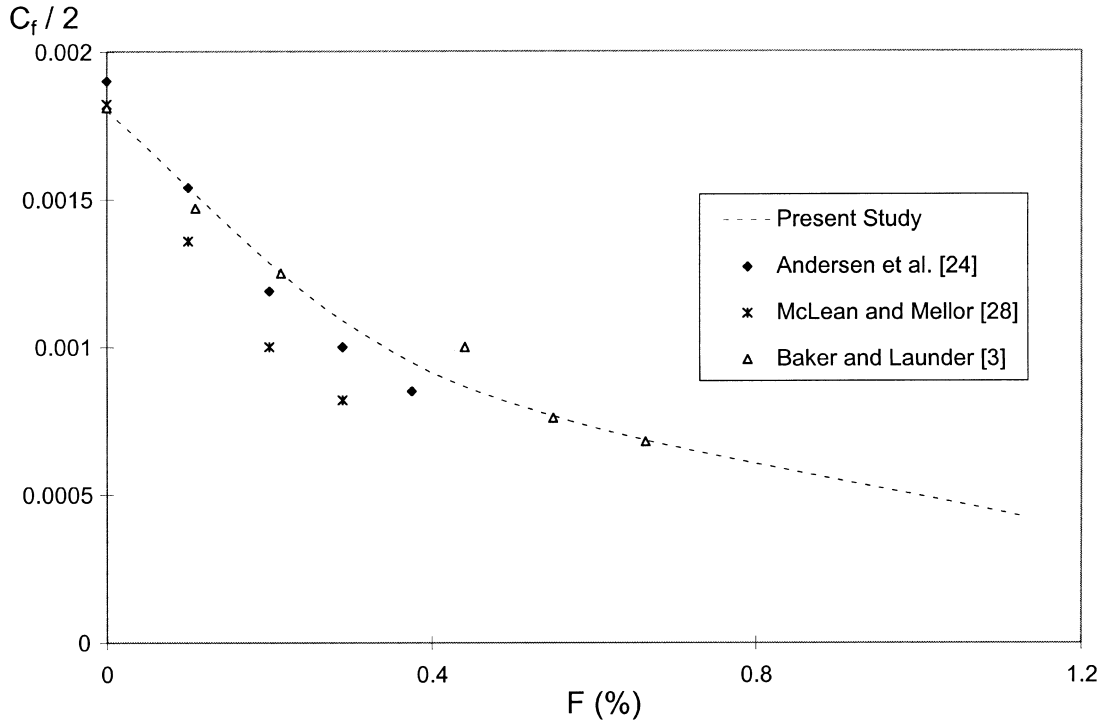

Fig. 14. Friction factors for different injection rates.

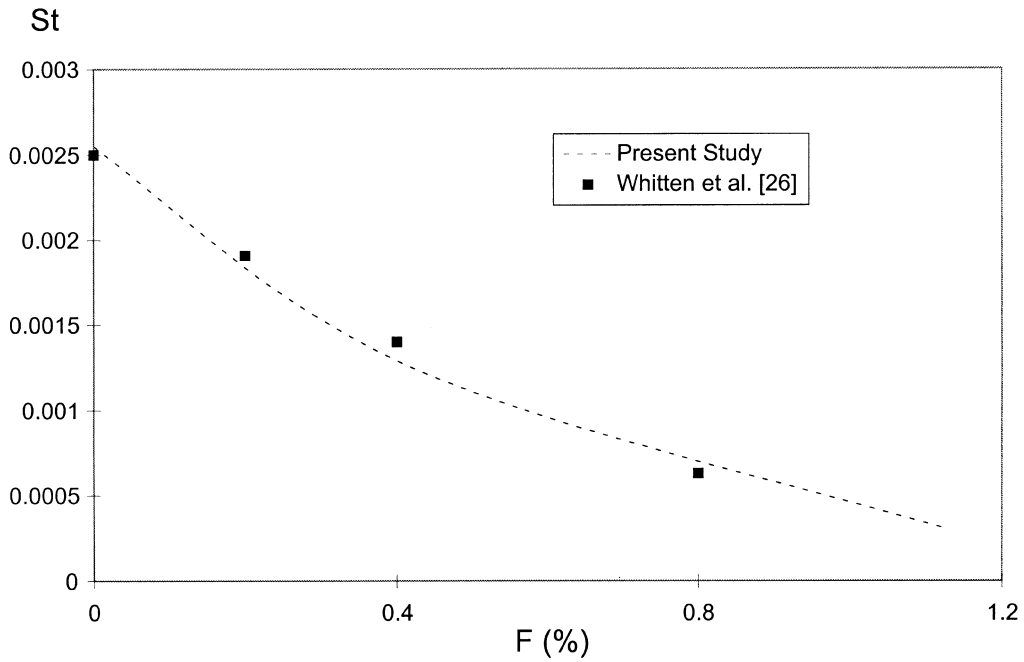

Fig. 15. Stanton numbers for different injection rates.

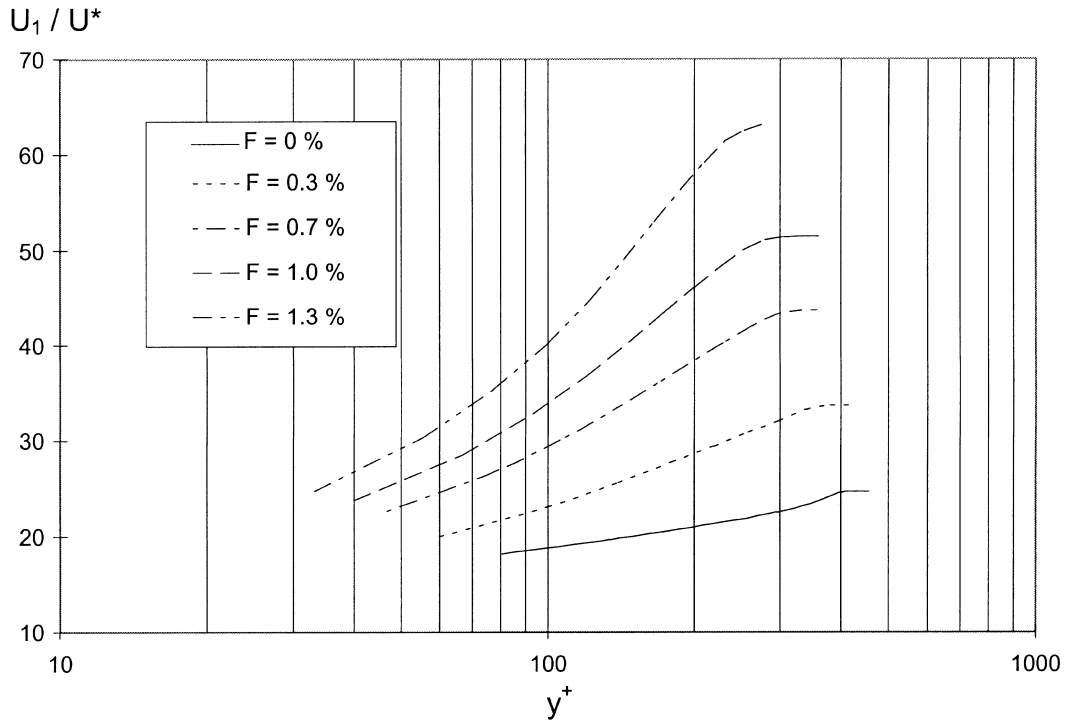

Fig. 16. Dimensionless velocity profile in the injection region for different injection rate.

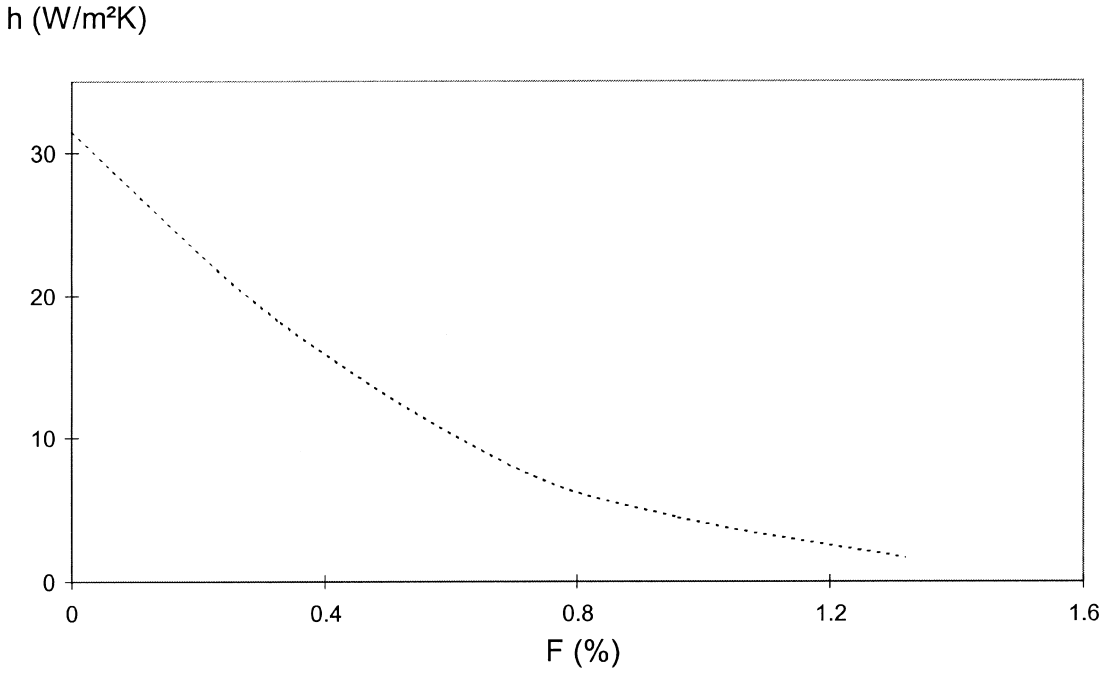

Fig. 17. Convective heat transfer coefficient for different injection rates (main flow temperature 100°C).

References

[1] R.J. Moffat, W.M. Kays, The turbulent boundary layer on a porous plate: experimental heat transfer with uniform blowing and suction, Int. J. Heat Mass Transfer 11, (1968) 1547–1566.

[2] R.L. Simpson, R.J. Moffat, W.M. Kays, The turbulent boundary layer on a porous plate: experimental skin friction with variable injection and suction, Int. J. Heat Mass Transfer 12 (1969) 771–789.

[3] R.J. Baker, B.E. Launder, The turbulent boundary layer with foreign gas injection. I—Measurement in zero pressure gradient, Int. J. Heat Mass Transfer 17 (1974) 275–291.

[4] P.N. Romanenko, V.N. Kharchenko, The effect of transverse mass flow on heat transfer and friction drag in a turbulent flow of compressible gas along an arbitrarily shaped surface, Int. J. Heat Mass Transfer 6 (1963) 727–738.

[5] R.L. Simpson, Characteristics of turbulent boundary layers at low Reynolds numbers with and without transpiration, J. Fluid Mech. 42 (1970) 769–802.

[6] T.N. Stevenson, Inner region of transpirated turbulent boundary layers, AIAA Journal 6 (1968) 553–554.

[7] A.P. Silva-Freire, An asymptotic solution for transpired incompressible turbulent boundary layers, Int. J. Heat Mass Transfer 31 (1988) 1011–1021.

[8] W.M. Kays, Heat transfer to the transpirated turbulent boundary layer, Int. J. Heat Mass Transfer 15 (1972) 1023–1044.

[9] R.B. Landis, F. Mills, The calculation of turbulent boundary layers with foreign gas injection, Int. J. Heat Mass Transfer 15, (1972) 1905–1932.

[10] R.M.C. So, G.J. Yoo, Low Reynolds number modeling of turbulent flows with and without wall transpiration, AIAA Journal 25 (1987) 1556–1564.

[11] G.A. Campolina Franca, Contribution à l'étude des écoulements parietaux avec effusion: application au refroidissement de parois, Ph.D. thesis, INSA de Lyon, France, 1996.

[12] G.A. Campolina Franca, C. Li, A. Lallemand, Simulaçao, por volumes finitos, do Escoamento turbulento incompressivel, nao-isotermico, no interior de um duto rectangular, com injecao, Proceedings of 15th CILANCE, Belo-Horizonte, Brazil, 1994, pp. 323–332.

[13] G. Tedeschi, G.A. Campolina Franca, A. Lallemand, Refroidissement de parois planes par transpiration: comparaison de différents modèles pour le calcul des échanges de chaleur, Proceedings of SFT Congress, Poitiers, France, 1995, pp. 206–211.

[14] G.A. Campolina Franca, G. Tedeschi, A. Lallemand, Turbulent incompressible flow within a channel with transpiration: solution of the coupled problem porous wall—main flow, Proceedings of 13th Brasilian Congress and 2nd Iberian American Congress of Mechanical Engineering, Belo Horizonte, Brasil, 1995.

[15] Y. Sun, I.S. Gartshore, M.E. Salcudean, An experimental investigation of film cooling, heat transfer coefficients using the mass/heat analogy, ASME, Journal of Heat Transfer 38 (1995) 851–858.

[16] C. Carcasci, B. Facchini, A numerical procedure to design internal cooling of gas turbine stator blades, Revue Generale de Thermique 35 (1996) 257–268.

[17] W.P. Jones, B.E. Launder, The prediction of laminarization with a two-equation model of turbulence, Int. J. Heat Mass Transfer 15 (1972) 301–314.

[18] V. Yakhot, S.A. Orszag, Renormalization group analysis of turbulence, I. Basic theory, J. of Sci. Comput. 1 (1986) 1–51.

[19] Y. Zhou, W.D. McComb, G. Vahala, Renormalization Group (RG) in turbulence: historical and comparative perspective, ICASE Report no 97–36, NASA, Langley, 1997.

[20] B.E. Launder, D.B. Spalding, The numerical computation of turbulent flow, Computer Methods Appl. Mech. Eng. 3 (1974) 269–288.

[21] S.V. Patankar, Numerical Heat Transfer and Fluid Flow, Hemisphere Publishing Corp., Washington, 1980.

[22] FLUENT, User's Guide Version 4.3, Fluents Inc, Lebanon, 1995.

[23] J.C. Rodet, G.A. Campolina Franca, P. Pagnier, R. Morel, A. Lallemand, Etude en soufflerie thermique du refroidissement de parois poreuses par effusion de gaz, Rev. Gén. Therm. 37 (1998) 123–136.

[24] P.S. Andersen, W.M. Kays, R.J. Moffat, Experimental results for the transpired turbulent boundary layer in an adverse pressure gradient, J. Fluid Mech. 69 (1975) 353–375.

[25] L.C. Squire, The constant property turbulent boundary layer with injection; a reanalysis of some experimental results, Int. J. Heat Mass Transfer 13 (1970) 939–942.

[26] D.G. Whitten, R.J. Moffat, W.M. Kays, Heat transfer to a turbulent boundary layer with non-uniform blowing and surface temperature, Proceedings of Fourth International Heat Transfer Conference, Versailles, France, 1970, paper FC8.8.

[27] J. Bellettre, F. Bataille, A. Lallemand, Study of a turbulent boundary layer with injection, Proceedings of ASME Fluids Engineering Division Summer Meeting, Symposium on Separated and Complex Flows, Vancouver, Canada, 1997.

[28] J.D. McLean, G.L. Mellor, The transpired turbulent boundary layer in an adverse pressure gradient, Int. J. Heat Mass Transfer 15 (1972) 2353–2369.

[29] J. Bellettre, F. Bataille, A. Lallemand, Non équilibre thermique d'une plaque poreuse refroidie par effusion, Proceedings of SFT Congress, Toulouse, France, 1997.